Shear alignment and realignment of sphere-forming and cylinder-forming block-copolymer thin films

Andrew P. Marencic,[1] Douglas H. Adamson,[2,3] Paul M. Chaikin,[4,5] and Richard A. Register[1,*]
[1]*Department of Chemical Engineering, Princeton University, Princeton, New Jersey 08544, USA*
[2]*Department of Chemistry, University of Connecticut, Storrs, Connecticut 06269, USA*
[3]*Polymer Program, Institute of Materials Science, University of Connecticut, Storrs, Connecticut 06269, USA*
[4]*Department of Physics, New York University, New York, New York 10003, USA*
[5]*Center for Soft Condensed Matter Research, New York University, New York, New York 10003, USA*
(Received 25 September 2009; published 21 January 2010)

In common with many other structured fluids, block copolymers can be effectively oriented by shear. This susceptibility to shear alignment has previously been shown to hold even in thin films, containing as few as two layers of spherical microdomains, or even a single layer of cylindrical microdomains. A phenomenological model has been proposed [M. W. Wu, R. A. Register, and P. M. Chaikin, Phys. Rev. E **74**, 040801(R) (2006)] to describe the alignment of such block-copolymer films, yielding the microdomain lattice order parameter as a function of shearing temperature, stress, and time. Here we directly test the central idea of that model, that the grains which are most misaligned with the shear direction are selectively destroyed, to reform in a direction more closely aligned with the shear. Films are first shear aligned from a polygrain state into a monodomain orientation and are then subjected to a second shear, at a variable stress (σ) and misorientation angle ($\delta\theta$) relative to the monodomain director, allowing the effects of σ and $\delta\theta$ to be independently and systematically probed. For both cylinder-forming and sphere-forming block copolymers, these experiments confirm the basic premise of the model, as the stress required for realignment increases monotonically as $\delta\theta$ becomes smaller. For a cylinder-forming block copolymer, we find that the characteristic stress σ_c required to realign cylinders from one monodomain orientation to another is indistinguishable from that required to generate a monodomain orientation from the polygrain state. By contrast, the hexagonal lattice of spheres requires a value of σ_c more than 3 times as high for reorientation than for generation of the initial monodomain orientation.

DOI: 10.1103/PhysRevE.81.011503 PACS number(s): 83.80.Uv, 68.15.+e, 68.55.am, 64.60.Cn

I. INTRODUCTION

Driven flow of complex fluids such as liquid crystals (LCs) or block copolymers (BCs) is interesting because there exists a coupling between the fluid's internal structure and the flow [1–3]. For instance, in nematic LCs, translational shear motions are coupled to the orientational motions of the molecules, which in turn can induce a flow [2]. Steady-state flow of LCs is well understood by the Eriksen [4,5], Leslie [6,7], and Parodi [8] (ELP) continuum theory, where the velocity vector of the fluid and the director describe the dynamics. According to this theory, the LCs will either assume a steady-state alignment angle with respect to the shear direction or develop an instability depending on the strain rate [2]. The transient behavior of start up of shear for strain rates that cause alignment to occur in nematics for different initial orientations was investigated and was also shown to conform to the ELP continuum model (neglecting elastic forces) [9–11].

Alignment of block copolymers by unidirectional shear is different from liquid crystals because block-copolymer domains are made up of many individual chains that can hop from one domain to another [12]. This complicates the ability to identify the mechanism by which alignment occurs: domain dissolution-reformation or grain rotation [13]. Extensive research has been reported on alignment of bulk BCs by unidirectional shear for different morphologies: spherical phase [14], cylindrical phase [15–17], and lamellar phase [18–20]. As with liquid crystals, there is a shear-rate dependence of the orientation of the domains, with cylinders and lamellae lying parallel or perpendicular to the shear direction [1,3] (although the theoretical prediction of perpendicular orientation for cylinders [16] and lamellae [20] has not been confirmed experimentally in unidirectional shear) and spheres disordering above a critical stress [21–23]. This diversity of behavior complicates the ability of researchers to deduce the mechanism by which shear alignment of block copolymers occurs.

When confined to thin films, surfaces play a large role such that the lamellae and cylinders will lie parallel to the surface [24,25] and the spherical phase will transition from a bcc lattice to a hcp lattice [26]. Our group has previously demonstrated that both sphere-forming and cylinder-forming block-copolymer thin films respond to a shearing field, orienting the cylinder axes [27,28] or the (10) lines of spheres [29,30] in the direction of the imposed shear. As expected, a minimum threshold stress (σ_{thresh}) is required to induce any alignment in the film [30]. Above this stress, the alignment quality—quantified by an orientational order parameter—increases quickly as stress increases and then reaches a plateau where the alignment is no longer dependent on stress [28,30]. A melting-recrystallization model was proposed to describe the observed behavior, where domain dissolution-reformation is assumed to be the mechanism by which shear-alignment occurs [28,30]. The model assumes an effective order-disorder transition temperature (T^*_{ODT}) that is a func-

*Corresponding author; register@princeton.edu

tion of the misorientation angle ($\delta\theta$) a given grain has with the shear direction, and the applied shear stress (σ) [28,30]

$$T^*_{\mathrm{ODT}}(\delta\theta) = T_{\mathrm{ODT}}[1 - (\sigma/\sigma_c)\sin^2(\alpha\delta\theta)], \quad (1)$$

where T_{ODT} is the order-disorder transition temperature of the block copolymer and α is a constant ($\alpha=3$ for spheres and $\alpha=1$ for cylinders because of lattice symmetry). The parameter σ_c is termed the critical stress, postulated to be independent of temperature, and related to the temperature-dependent σ_{thresh} by $\sigma_{thresh}=\sigma_c(1-T/T_{\mathrm{ODT}})$ [31]. If the temperature is high enough and a grain's misorientation is large enough, the grain will "melt" and subsequently "recrystallize" in an orientation dictated by the shear direction. The rate of melting-recrystallization of a grain is assumed constant [28,30]

$$\partial R/\partial t = \Gamma(T^*_{\mathrm{ODT}} - T)/T_{\mathrm{ODT}}, \quad (2)$$

where R is the area of a grain and Γ is a rate constant that determines how quickly the limiting alignment is reached. The total grain population is conserved such that $\int_0^{\pi/\alpha} R(\delta\theta,t)d\delta\theta=$const. The orientational order parameter can then be calculated from Eq. (2) [28,30]

$$\psi_{2\alpha} = D\frac{\int_0^{\pi/\alpha} R(\delta\theta)\cos(2\alpha\delta\theta)d\delta\theta}{\int_0^{\pi/\alpha} R(\delta\theta)d\delta\theta}, \quad (3)$$

where $\psi_{2\alpha}$ is the orientational order parameter that is measured in the experiments (ψ_2 for cylinders and ψ_6 for spheres) and D is a Debye-Waller-like factor related to the uncertainty in determining the microdomain position. For long cylinders, the uncertainty in locating their axes is insubstantial ($D=1.0$) [32], but for spheres, the uncertainty in locating the sphere center by atomic force microscopy leads to $D=0.85$ for the polymer and imaging system employed herein [33]. The melting-recrystallization model thus contains two material parameters which are unknown *a priori*: σ_c and Γ. For the sphere-forming block copolymer used in this study, these were determined to be $\sigma_c=1900$ Pa and $\Gamma=0.01$ s^{-1} by shearing a random distribution of grains at various time-temperature combinations and evaluating ψ_6 (refit using data from Ref. [30] and additional data). Experimental data showed excellent agreement with the model, which is somewhat surprising considering the model's simplicity. Parameter values for the cylinder-forming block copolymer used in this study have not been published and will be covered in the next section, although another cylinder-former [polystyrene-block-poly(*n*-hexylmethacrylate)] was previously tested and shown to conform to the melting-recrystallization model [28].

The model was previously tested against experiments where the initial condition was an ensemble of grains of all orientations, leading to stress being the one independent variable for a given shearing time and temperature. The angular dependence of the grain response is averaged over the entire ensemble, obscuring the dependence on $\delta\theta$. Here we directly test the melting-recrystallization model's idea that melting is dependent on σ and $\delta\theta$ independently by first macroscopically orienting a specimen by shear, then shearing the sample a second time in a different direction. By using a constant stress rheometer with a parallel-plate attachment, we obtain continuous gradients in both $\delta\theta$ and σ over the sheared area, allowing the effects of $\delta\theta$ and σ to be independently mapped out in a single experiment.

II. EXPERIMENT

A. Materials

The sphere-forming [29,30,33,34] and cylinder-forming [27,28,35] block copolymers used in this study are polystyrene-block-poly(ethylene-*alt*-propylene) diblocks (PS-PEP) of different PS volume fractions, synthesized through sequential living anionic polymerization of styrene and isoprene [22,32] followed by selective saturation of the isoprene block [36]. Both polymers have been described previously in the references noted, though the sample codes differed slightly from those used here. The number-average block molecular weights for the sphere-forming block copolymer (PS-PEP 3/23) are 3.3 kg/mol for PS and 23.1 kg/mol for PEP. For the cylinder-forming block copolymer (PS-PEP 4/13), which was saturated with deuterium instead of hydrogen (not explicitly noted in [27,28,35]), the number-average molecular weights are 4.3 kg/mol for PS and 12.6 kg/mol for PEP (hydrogenous equivalents, i.e., not accounting for the extra mass of deuterium over hydrogen). Small-angle x-ray scattering (SAXS) was used to determine the bulk morphology of PS-PEP 3/23 to be spheres configured in a bcc lattice, with $T_{\mathrm{ODT}}=121\pm2$ °C [22]. Using the same procedure, the cylindrical morphology was confirmed for PS-PEP 4/13 with $T_{\mathrm{ODT}}=144\pm2$ °C [37]. In thin films, the minority PS block wets the substrate (silicon wafers, purchased from Silicon Quest International, were prewashed with toluene and dried under flowing nitrogen, leaving the native oxide intact), with layers of PS microdomains embedded in the PEP matrix on top of this brushlike wetting layer [27]. The spheres in PS-PEP 3/23 arrange into a hexagonal configuration in thin films [29], while the cylinders in PS-PEP 4/13 adopt a configuration parallel to the substrate because of large surface energy differences between the blocks [32].

B. Sample preparation

The block copolymers were applied to one half of a 3″ silicon wafer by spin coating from a dilute solution (~1–2% by weight). By manipulating the spin speed and concentration, the thickness of the film, and thus the number of layers of microdomains, can be controlled. A monolayer of cylinders (30 nm) was used in these experiments, but a trilayer of spheres (78 nm) was employed, since a monolayer of spheres is intrinsically isotropic and will not shear align [29] (unless the block copolymer has a composition near the sphere-cylinder boundary [38], which our block copolymers do not). No noticeable difference is seen between a bilayer and a trilayer of spheres in their alignment-stress response [39]. All films were spun to ensure an integer number of layers, so no

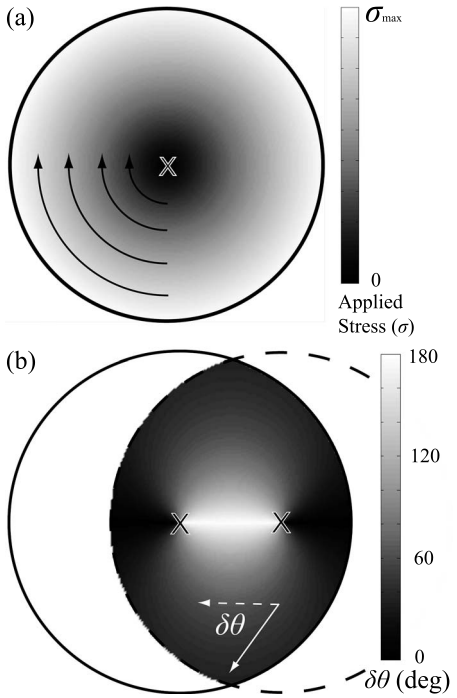

FIG. 1. Schematic of the geometry of the parallel-plate rheometer in single- and double-shear experiments indicating (a) the applied stress imparted to the block-copolymer thin film at various points from the rotation axis (×) and (b) the angular difference ($\delta\theta$) between the two shear directions calculated at each point within the overlap region. See supplement material for a color-scale version of this figure (Ref. [43]).

discernable islands or holes were present before shearing. Both the first and second shears were done using a constant stress rheometer (Anton Paar MCR-501) using a 25 mm parallel-plate attachment. A coated wafer is secured to the rheometer's Peltier heater, followed by the application of a top layer of polydimethylsiloxane (PDMS) oil (room-temperature kinematic viscosity of 1.0×10^6 cS from Gelest). The parallel plate is then lowered into position until the thickness of the oil is ~0.2 mm. The entire system is then heated to temperature, allowed to equilibrate for 5 min, and then sheared at a constant stress for 30 min. The parallel-plate attachment allows for continuous variation in stress along the radial direction in the film; since the PDMS oil is essentially Newtonian, the relation is given by

$$\sigma = \frac{r}{R}\sigma_{\max}, \tag{4}$$

where r is the distance from the rotation axis, R is the radius of the parallel plate, and σ_{max} is the stress at the edge of the plate, which is set during the experiment [see Fig. 1(a)]. The stress used here is large enough that most of the sample will be aligned in the direction of shear (above the plateau stress of ~600 Pa for PS-PEP 3/23 and ~400 Pa for PS-PEP 4/13, where alignment quality becomes essentially independent of stress). For PS-PEP 3/23, σ_{max}=3200 Pa and for PS-PEP 4/13, σ_{max}=1600 Pa. Following the first shear, the sample is translated relative to the rotation axis, resecured to the heater, and sheared again to create a continuous gradient in the angular difference between the two shearing directions [see Fig. 1(b)]. Following the shearing, the PDMS oil is removed by "sponging" with a cross-linked PDMS pad.

C. Imaging and analysis

The thin films are imaged in real space using a Digital Instruments (now Veeco) Dimension 3000 atomic force microscope (AFM) in tapping mode with uncoated Si tips (Veeco) having a cantilever length of ~125 μm, spring constant of ~40 N/m, and resonant frequency of ~300 kHz. At room temperature, the elastic modulus difference between the rubbery PEP and the glassy PS is sufficient to detect in phase mode without destruction of the film. Quantitative analysis of the images is done using software written in Interactive Data Language (IDL). The analysis for the spheres and cylinders is different so each will be discussed individually below.

1. Cylinder analysis

The real-space image (2.5×2.5 μm^2) is Fourier filtered with an annulus convoluted with a Gaussian blur to remove high- and low-frequency noises [32]. The director of the cylinder is found in real space by determining local x and y gradients, the direction of steepest decent in pixel intensity [32]. The cylinder (axis) orientation is then this direction plus 90°. The alignment quality is quantified using the orientational order parameter (ψ_2) defined here

$$\psi_2 = \langle\cos[2(\theta-\theta_0)]\rangle = \langle\cos(2\delta\theta)\rangle, \tag{5}$$

where θ is the orientation of a cylinder, θ_0 is the direction of shear, and the factor of 2 is required for the twofold symmetry of the lattice. The average is taken over all pixels in the image. Figure 2(a) shows an image of an unaligned film, which clearly shows one grain boundary running diagonally.

To increase the area covered per image (with the same 512×512 pixel resolution), moiré interference patterns were used to determine the orientation of the cylinders. A moiré pattern is formed from the interference between the AFM scan lines and the underlying cylinders and is most easily observed when the ratio of microdomain lattice spacing (distance between cylinders, P_L) to grid spacing (distance between AFM scan lines, P_G) is approximately equal to an integer (up to 3) [40]. With $P_L/P_G\cong1$ and P_L=20 nm, moiré patterns are observed in 8.5×8.5 μm^2 images—a tenfold increase in area coverage over the real-space images. Reference [40] presents equations that describe the lattice orientation (θ) as a function of moiré line orientation (ϕ) and spacing (P_M), both of which are easily determined from the Fourier transform of the moiré pattern. The intensity of the peaks in Fourier space is related to the fractional coverage of a grain within the image such that the angular distribution of grains relative to the shearing direction, $R(\theta_i-\theta_0)$, can be determined. The orientational order parameter can then be evaluated

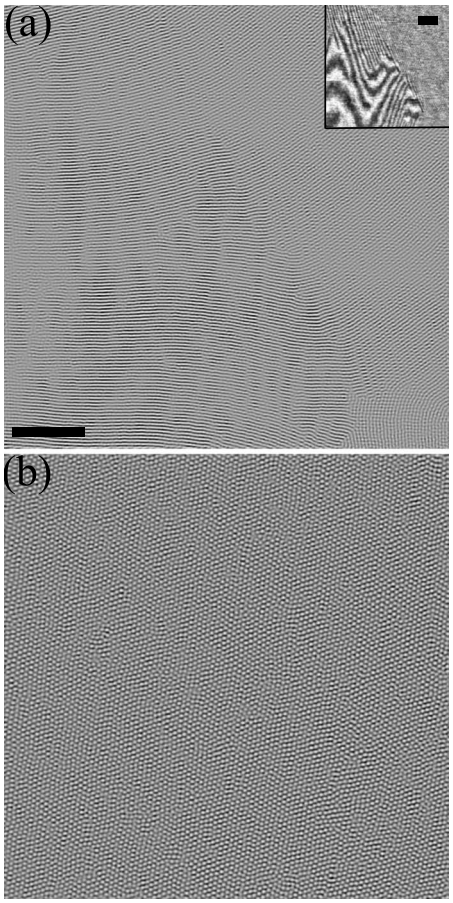

FIG. 2. (a) Real-space filtered image of unaligned cylinder-forming PS-PEP 4/13. Inset is the moiré interference pattern of the same area, showing strong bands when the AFM scan direction is in same direction as the cylinder axis (horizontal). (b) Real-space filtered image of aligned (~9° off vertical) sphere-forming PS-PEP 3/23. Scale bars are 400 nm.

$$\psi_2 = \frac{\sum_i R(\theta_i - \theta_0)\cos[2(\theta_i - \theta_0)]}{\sum_i R(\theta_i - \theta_0)} = \frac{\sum_i R(\delta\theta_i)\cos[2(\delta\theta_i)]}{\sum_i R(\delta\theta_i)}, \tag{6}$$

where the sum is taken over some discrete division of θ (here, divisions were in 1° increments). Because of the difficulty in observing a moiré pattern when the scan direction is perpendicular to the cylinder director, multiple images were taken over the same area at different scan angles and the full angular distribution was pieced together. An example of a moiré pattern is given in the inset in Fig. 2(a): strong moiré lines appear when the cylinder axis is aligned with the fast AFM scanning direction (horizontal) and disappear when the cylinder axis turns toward vertical.

2. Sphere analysis

Real-space images are first stretched to correct for thermal drift and piezo drift then Fourier filtered as for real-space images of the cylinders. The position of each sphere in real space is found using a particle-finding algorithm [41]. A Delaunay triangulation is then done to find nearest neighbors, locate dislocations, and determine bond vectors. The orientational order parameter (ψ_6) can then be calculated

$$\psi_6 = \langle \cos[6(\theta - \theta_0)] \rangle = \langle \cos(6\delta\theta) \rangle \tag{7}$$

where θ is the orientation of a bond vector, θ_0 is the direction of shear, and the factor of 6 is required for the sixfold symmetry of the lattice. An example of a filtered real-space image is shown in Fig. 2(b) with the aligned spheres clearly shown as white spots on a dark background. The average is taken over all bond vectors in the image. Uncertainty in the sphere position by AFM limits the orientational order parameter of a defect-free film to $\psi_6(\max) = D = 0.85$ [33].

The position of the rotation axis must also be determined to accurately calculate the imposed stress and the shear direction. This is done using scratches made around the edge of the rheometer tool, whose positions are fit to a circle. The shear direction and stress are then found from the locations where AFM images were taken relative to the rotation axis.

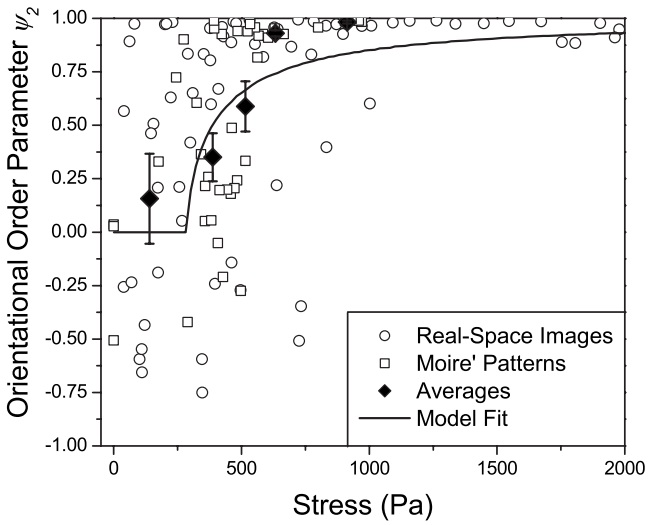

FIG. 3. Orientational order parameter as a function of stress for a monolayer of cylinder-forming PS-PEP 4/13 sheared at 135 °C for 30 min. Open circles are from real-space AFM images, open squares are from moiré interference patterns, and filled diamonds are averages of the open squares in 150 Pa bins, except for the lowest-stress (0–300 Pa) and highest-stress (>750 Pa) bins. Error bars on these averages represent ±1 standard deviation of the mean. Solid line is the melting-recrystallization model fit to the open squares.

III. RESULTS AND DISCUSSION

A. Single shear cylinders

Figure 3 shows the relationship between ψ_2 (calculated using both real-space images and moiré patterns) and the applied shear stress for a single shear of the PS-PEP 4/13 (from an initially polygrain state, as prepared) at 135 °C for 30 min. At high stresses (>600 Pa), alignment of the cylindrical microdomains with the shearing direction is observed. As expected, below a certain stress, no alignment was

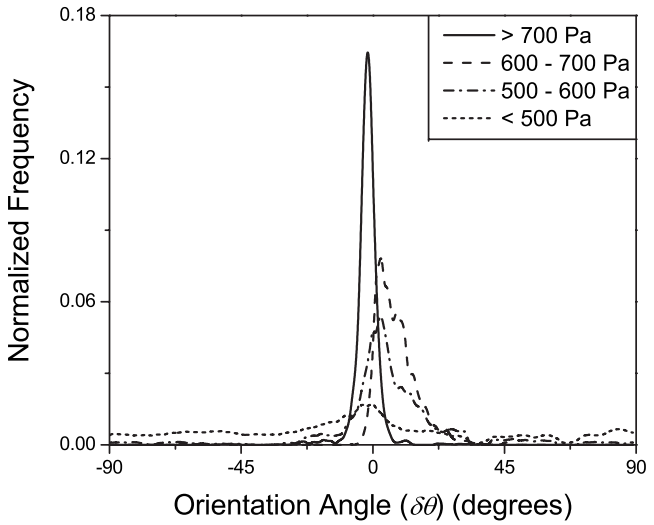

FIG. 4. Angular distribution of PS-PEP 4/13 grains with respect to the shear direction (modulo 180°) at different applied shear stresses after shearing for 30 min at 135 °C. A relatively flat distribution is observed at low stresses, but at higher stresses the grains most misaligned from the shear direction are progressively destroyed, making the distribution narrower as stress increases.

observed—only grains of all orientations. Determination of this stress, σ_{thresh}, and the subsequent transition region was difficult using real-space images because the correlation length of the cylinders in PS-PEP 4/13 after 30 min at 135 °C is ~10 μm [32], larger than the AFM scan area, leading to a very large scatter of ψ_2 (± 1.0) at low stress. Nonetheless, attempts were made to fit the melting-recrystallization model to the results obtained using real-space images. A narrow transition region (deduced from the data since there appears to be a sudden transition from unaligned to aligned in the images as stress is increased) indicates that the melting-recrystallization process is saturated with time (longer shearing will not lead to better ordering), which limits what can be said about the rate constant: $\Gamma > 2\ s^{-1}$. The large scatter at low stress also limits what can be said about the critical stress. The value for σ_{thresh} could be anywhere up to 500 Pa, which translates to $\sigma_c < 23\,000$ Pa. Figure 3 also contains isolated data points at higher stresses ($\sigma > 500$ Pa) from real-space images that had a lower orientational order parameter than expected, based on images from other areas sheared at a similar stress. For PS-PEP 4/13, the shearing process can be harsh enough to rip the block copolymer from its wetting layer, creating holes within the film [28]. Near a hole, the cylinder director will tend to orient perpendicular to the edge; our observations indicate that this orientation persists over approximately the unsheared grain size or ~10 μm for PS-PEP 4/13. We believe that the outlying data points in Fig. 3 came from images taken "close to" a hole (outside the actual image, but within 10 μm).

Using moiré interference patterns (open squares in Fig. 3) to determine the orientational order of the PS-PEP 4/13 film allowed for a tenfold increase in imaging area, bringing the correlation length to the same size as the imaging window. It also allowed us to easily observe any holes present and restrict our imaging to regions >10 μm from any film-hole boundary. Satisfyingly, the moiré results show no "outliers" (no points with small ψ_2 at $\sigma > 500$ Pa). The increase in imaging area also resulted in reduced scatter of the data near σ_{thresh}. As each image is an individual snapshot of the entire ensemble, averaging the data from the moiré patterns allowed for better visualization of the trend and estimation of the error as stress increases (Fig. 3). The reduced scatter in the moiré patterns also allowed for better determination of the critical stress compared to the real-space images: $\sigma_c = 13000 \pm 2000$ Pa using a Levenberg-Marquardt algorithm to minimize χ^2. The steep transition in ψ_2 still limits Γ to be greater than 2 s^{-1}. Note that the final approach of ψ_2 toward unity with increasing stress is faster in the data than in the model calculation; this is largely set by the functional form postulated for T^*_{ODT} in Eq. (1). While more complex functional forms could provide better fits to the data, we focus here on the behavior around the transition from unaligned to aligned films. One can view the angular distribution [$R(\delta\theta)$—approximately ten moiré patterns averaged for each distribution in Fig. 4] to see the sharp transition from a nearly flat distribution below 500 Pa to highly aligned grains at 700 Pa. In the transition region, grains at the greatest mismatch to the shear direction are annihilated and a narrow distribution centered near $\delta\theta = 0$ forms which sharpens with increasing stress, in agreement with the melting-recrystallization model.

B. Double-shear cylinders

Figure 5 shows the geometry of the double-shear experiment. In Fig. 5(a), the dashed circle is the outline of the rheometer plate during the first shear (135 °C for 30 min with $\sigma_{\max} = 1600$ Pa), with a diameter of 25 mm centered at +. Outside of this circle, no shear was imposed so no alignment is observed. Within the dashed circle, at stresses above the plateau stress (~600 Pa), the grains are macroscopically oriented along the shear direction. For the second shear, the rotation axis is translated to the left (new position at ×). The orientational order parameter, shown as the background shading in Fig. 5(a), is then recalculated using the second rotation axis (×) as the origin, though the actual film orientation is unchanged from the first shear. Inside the dashed circle are two lobes of white where the grains are already aligned with the second-shear direction and two lobes of black where the grains are initially anticorrelated (~90°) with the second-shear direction. The area in the middle of the dashed circle (center shown with a +) is where the first-shear stress was not large enough to orient the grains so the orientational order parameter is equal to zero on average. The solid circle is the outline of where the second shear will take place. The lozenge-shaped intersection of these two circles—the "realignment" region—is the area of interest. Of particular interest will be the change in the dark anticorrelated lobes as the stress is increased [as one moves outward from the rotation axis of the second shear (×) along the initially anticorrelated lobes].

Based on the melting-recrystallization model, we can anticipate what the resulting distribution of orientational order parameters will look like for a given maximum shearing

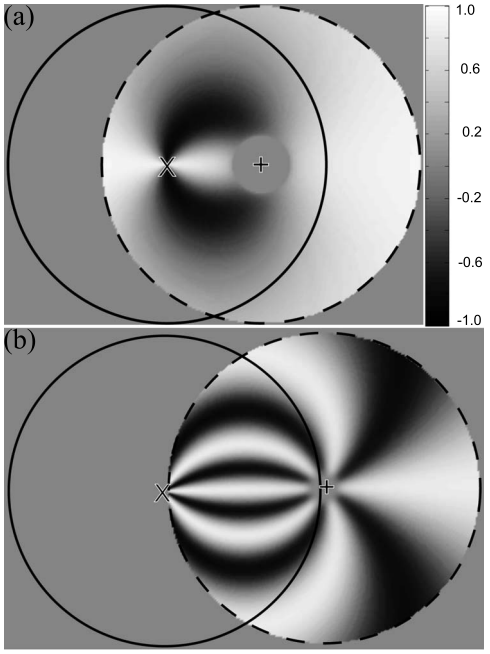

FIG. 5. Shading representing the model predictions of the initial orientational order parameter ($\psi_{2\alpha}$) distribution before the second shear for both the (a) cylinder-forming (first shear at 135 °C for 30 min at $\sigma_{\max}=1600$ Pa) and (b) sphere-forming (first shear at 85 °C for 30 min at $\sigma_{\max}=3200$ Pa) PS-PEP block-copolymer thin films. Dashed circle represents outline of rheometer tool for first shear centered at +, while the solid circle represents the outline for what will be the second shear centered at ×. See supplement material for a color-scale version of this figure (Ref. [43]).

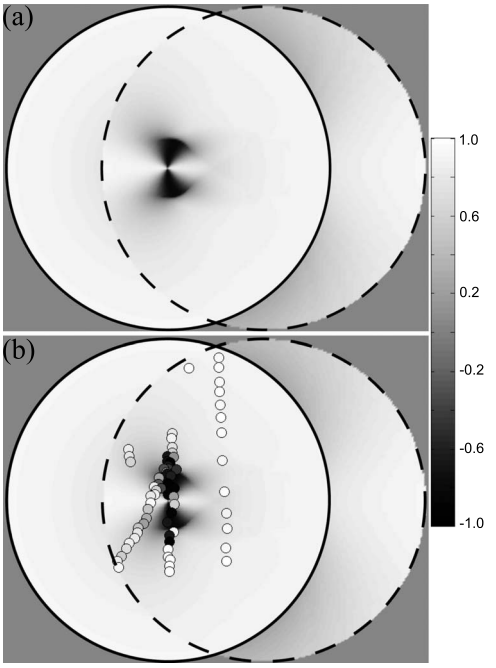

FIG. 6. Results for a cylinder-forming block-copolymer thin film aligned in double-shear (both shears done at 135 °C for 30 min at $\sigma_{\max}=1600$ Pa) with (a) showing the expected orientational order parameter relative to the second-shear direction, ψ_2 (shading according to the scale bar), using the parameters determined from the single-shear fits, and (b) showing experimental data as points with the model predictions as background shading. The shading of the points is the measured ψ_2 obtained from real-space AFM images; the center of each data point (shown 2 orders of magnitude larger in diameter than the actual image) corresponds with the location of the AFM image, whose position dictates the applied stress and difference in angle from the orientation imparted by the first shear. See supplement material for a color-scale version of this figure (Ref. [43]).

stress, shearing temperature, and shearing time (1600 Pa, 135 °C, and 30 min, respectively). This is shown in Fig. 6(a). Outside of the second-shear region (solid circle), no changes occur since there was no additional shearing done on these areas. Inside the second-shear region but outside the first-shear region (dashed circle), the distribution would look as it would for a single shear from an initially polygrain state, with ordering along the shear direction (confirmed using AFM images). Within the intersection region, the anticorrelated lobes are expected to be small since $\sigma_{thresh}=300$ Pa at 90° and Γ is so large; the majority of the intersection region should be oriented with the second-shear direction. Real-space AFM images were taken within the intersection region to determine how well these melting-recrystallization model predictions describe the actual system (moiré interference patterns were not required because areas below σ_{thresh} would still be aligned with the first-shear direction, clearly revealing the value of σ_{thresh}). Figure 6(b) shows the measured orientational order parameters extracted from these images. The center of the data point is where the image was taken, although the image width is 2 orders of magnitude smaller than the diameter of the data point. The shading of the point reflects the orientational order parameter of the image. Excellent agreement is achieved throughout the intersection region. Notably, the locations of the sharp transitions in ψ_2 (from nearly −1 to +1) that occur along the ±90° contour line (angles measured relative to the line connecting the rotation axes for the two shears, × and +) are precisely captured. To better illustrate the melting-recrystallization model's ability to describe the realignment process, Fig. 7 shows a one-dimensional (1D) plot of ψ_2 versus stress for data points within the range $\delta\theta=70\pm10°$, as well as the model fit at $\delta\theta=70°$. The experimental data confirm the location of σ_{thresh} and the steep transition confirms that the shear is saturated with time ($\Gamma>2$ s^{-1}). Again, averages were taken over stress intervals to showcase the trend. As in Fig. 3, data asymptote toward $\psi_2=1$ more quickly than the model prediction. In the transition region from unaligned to aligned, near 400 Pa, close examination of Fig. 7 reveals that the match between model and data could be improved by allowing for a modestly higher value of σ_c in the second shear, but the difference is within the uncertainty in the value of σ_c obtained from fitting the single-shear data (Fig. 3). We will return to this point below.

C. Double-shear spheres

An analogous study was conducted with the sphere former, PS-PEP 3/23. Figure 5(b) represents the initial condition of the orientational order parameter ψ_6 before the sec-

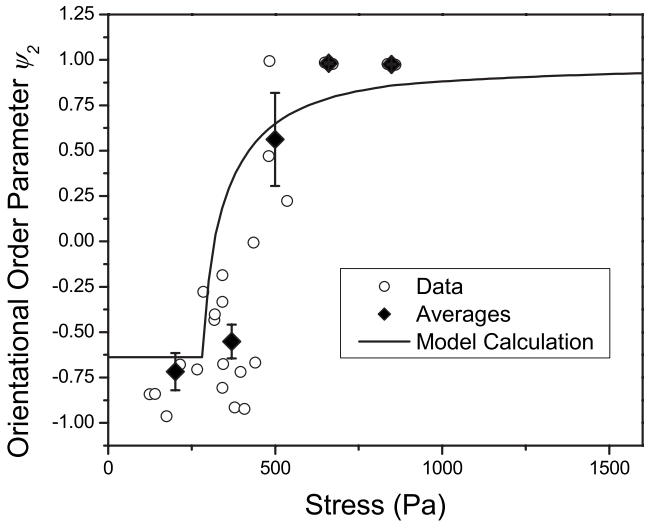

FIG. 7. Orientational order parameter of double-sheared (both at 135 °C for 30 min at $\sigma_{max}=1600$ Pa) cylinder-forming block-copolymer thin film as a function of the second-shear stress, for $\delta\theta=70°$. Open circles are the experimental data measured using real-space AFM images (at $\delta\theta=70°\pm10°$) and filled diamonds are averages taken over 150 Pa bins, except for the lowest-stress (0–300 Pa) and highest-stress (>750 Pa) bins. Error bars on these averages represent ±1 standard deviation of the mean. Solid line is the fit to the melting-recrystallization model ($\delta\theta=70°$) using parameters obtained from single-shear results from an initially polygrain state.

ond shear was done, with the dashed circle representing the first shear (85 °C for 30 min with $\sigma_{max}=3200$ Pa) and the solid circle representing where the second shear will take place. Again, the areas of particular interest are the bands within the intersection region of the two circles which are initially anticorrelated with the second-shear direction (±30° and ±90°), shown in black. The increased number of lobes here compared to the PS-PEP 4/13 is due to the increased symmetry of the hexagonal lattice over the twofold symmetry of the cylinders. The reduced size of the unaligned portion at the center of the first shear is due to the reduced σ_{thresh} value (200 Pa) relative to the maximum stress. Outside this small area, all spherical microdomains within the dashed circle are aligned with the shear direction, such that the (10) lines of spheres are oriented tangential to the rotation axis (confirmed using real-space AFM images).

Figure 8(a) represents the expected orientational order parameter distribution following the second shear (85 °C for 30 min with $\sigma_{max}=3200$ Pa), calculated using parameters derived from single-shear experiments on initially polygrain specimens. Because of the low σ_{thresh} value and the low Γ value (obtained from shears of different duration [30]) compared to PS-PEP 4/13, the transition region from unaligned to highly aligned spans a greater stress range and should be observable when probed using AFM. We find, however, that a larger-than-expected area was not reoriented and is instead still aligned with the first-shear direction. Figure 8(b) shows the experimental data, where the transitions occur at stresses larger than those calculated in Fig. 8(a). To better illustrate this subtle difference, the same data are presented as 1D plots, ψ_6 as a function of the second-shear stress, in Figs. 8(c)–8(f). Each plot contains experimental data and the model calculations from Fig. 8(a) as dashed curves. The error bars in these plots reflect both uncertainty in geometry (uncertainty in location of the imaging site and rotation axis lead to uncertainty in the shear direction and thus the measured order parameter) and the presence of isolated dislocations (which have a linear effect on the measured order parameter [33] and are present at variable levels across the images). The data along the $-26\pm2°$ contour line in Fig. 8(c) best illustrate the deficiencies of the calculation using the single-shear parameters, where σ_{thresh} appears to occur at a much higher stress—an increase by a factor of 3. If all double-shear data are refit to the model, retaining the same initial distribution as calculated in Fig. 5(b), we find a larger value for $\sigma_c=6100\pm200$ Pa. The background shading in Fig. 8(b) reflects the model calculation using $\sigma_c=6100$ Pa for the second shear; note the subtle differences in shading intensity from Fig. 8(a). With the larger value of σ_c, calculated values of ψ_6 in the intersection region are lower: the applied stress does not achieve as much realignment as initially expected. Figures 8(c)–8(f) also include these model calculations ($\sigma_c=6100$ Pa) as solid curves. By adjusting σ_c upwards for the second shear (from 1900 to 6100 Pa), the model represents the experimental data much better.

To evaluate the rate constant, Γ, a short-time shearing experiment was done. The first shear was the same as in Fig. 8 ($\sigma_{max}=3200$ Pa, $T=85$ °C, 30 min), while the second shear was for a shorter time ($\sigma_{max}=3200$ Pa, $T=85$ °C, 5 min). Figure 9(a) shows the experimental data in the same format as before, with the first shear inside the dashed circle centered at + and the second shear inside the solid circle centered at ×. The areas of greatest interest here are the initially anticorrelated lobes near the center of the first shear so that the movement of the transition region with time can be monitored. Fitting these data to the melting-recrystallization model and allowing Γ to float (but fixing $\sigma_c=6100$ Pa for the realignment) yields $\Gamma=0.02\pm0.01$ s^{-1}, within the fit uncertainty of $\Gamma=0.01$ s^{-1} determined from the data in Fig. 8. The data sets were again converted to 1D plots as a function of the stress applied during the second shear [Fig. 9(b)] and as a function of the angular difference between the two shearing directions [Fig. 9(c)], where either $\Gamma=0.01$ s^{-1} (dashed curve) or $\Gamma=0.02$ s^{-1} (solid curve) was employed for the second shear. Again, given the complexity of the transition behavior, our simple model gives a surprisingly good representation of the observed trends. Both calculated curves capture the transitions from anticorrelation to correlation as a function of position within the double-sheared region and are similar in overall fit quality, indicating that a common value of $\Gamma=0.01-0.02$ s^{-1} can be used to model both the orientation of spherical microdomains from an initially polygrain state as well as their realignment from one orientation to another.

We attribute the increased stress needed to reorient a grain in the shear-aligned sphere-forming block-copolymer thin films to the need to nucleate a "molten" (disordered) region within the monodomain structure. In a single-shear experiment, the initial condition is that of small grains with all orientations. The shearing process will then grow grains in

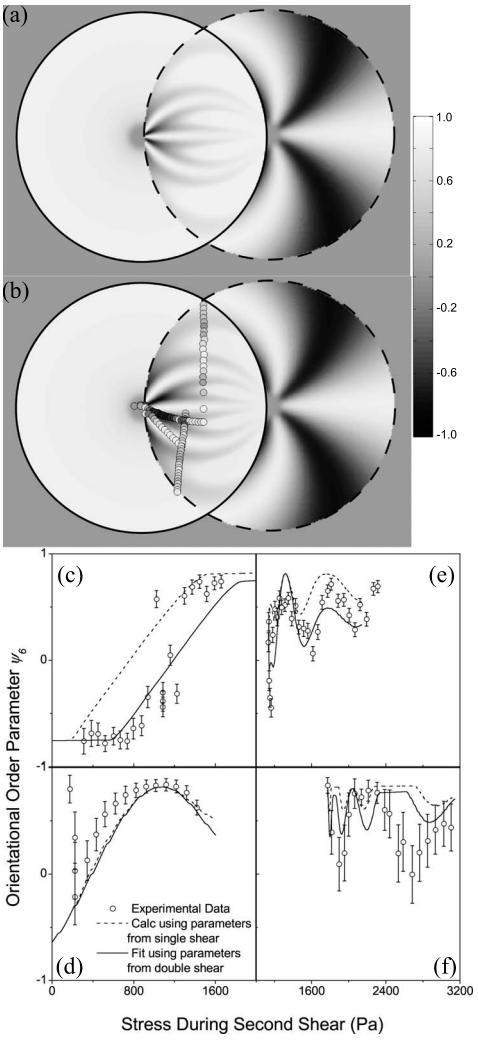

FIG. 8. Results for a sphere-forming block-copolymer thin film aligned in double shear (both shears done at 85 °C for 30 min at $\sigma_{max}=3200$ Pa) with (a) showing the expected orientational order parameter, ψ_6 (shading according to the scale bar), using the parameters determined from the single-shear fits, and (b) showing experimental data with the model adjusted to have a larger critical stress (σ_c) value for the second shear as background shading. The shading of the experimental data is the measured orientational order parameter obtained from real-space AFM images and the placement of the data point (2 orders of magnitude larger in diameter than the actual image width) dictates the applied stress and difference in angle from the prealigned orientation. Each set of points taken along a line is then converted to a 1D plot as a function of applied stress during the second shear: (c) upper data set emanating from the center of the second shear (along the $-26\pm2°$ contour line), (d) lower data set emanating from the center of the second shear—panel shares stress axis with (c), (e) lower vertical data set, and (f) upper vertical data set—panel shares stress axis with (e). Each 1D plot includes experimental data with error bars, the melting-recrystallization model calculations using single-shear parameters only (dashed curves) and model calculations using a larger critical stress (σ_c) value for the second shear (solid curves) with a common legend found in (d). Error bars represent estimates of ±1 standard deviation of the uncertainty in ψ_6 for the individual points. See supplement material for a color-scale version of this figure (Ref. [43]).

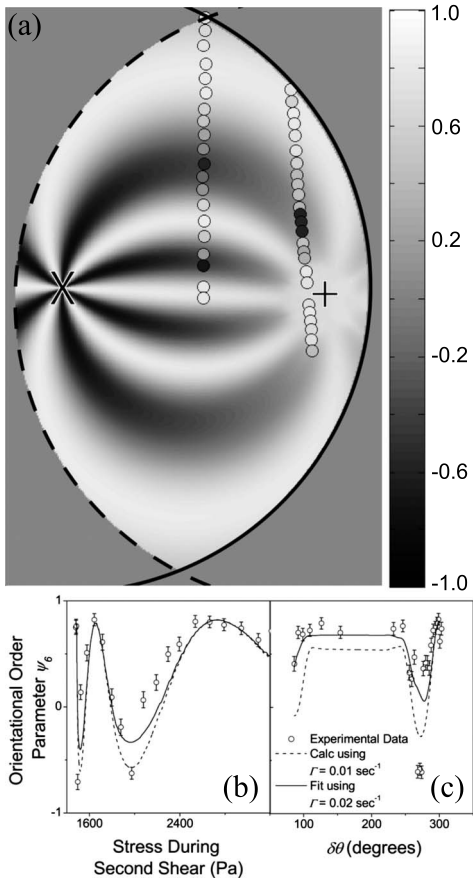

FIG. 9. Results for a sphere-forming block-copolymer thin film aligned in double-shear (first shear done at 85 °C for 30 min at $\sigma_{max}=3200$ Pa and the second shear done at the same conditions for only 5 min). For (a), the dashed curve represents the outline of the rheometer tool for the first shear and the solid curve the outline for the second shear. The background shading represents melting-recrystallization model predictions for ψ_6 using an increased σ_c (6100 Pa) and increased Γ (0.02 s^{-1}) for the second shear. Small circles are the experimental data measured using real-space AFM images, with their shading representing the measured orientational order parameter. Each set of points taken along a line is then converted to a 1D plot as a function of (b) stress applied during the second shear and (c) angular difference between the two shear directions. Each 1D plot includes experimental data with error bars, the melting-recrystallization model calculations using the smaller Γ (0.01 s^{-1}, dashed curves), and model predictions using a larger Γ value for the second shear (solid curves) with a common legend found in (c). See supplement material for a color-scale version of this figure (Ref. [43]).

the correct orientation while simultaneously destroying grains in incorrect orientations, processes which proceed from grain boundaries. In a double-shear experiment, however, the initial condition is that of a monodomain, misaligned to the shear direction, without grain boundaries. Reorientation thus requires the nucleation of a molten region, from which grains in the shear direction can grow.

The enhanced stress in the double-shear experiment thus represents the extra stress required to nucleate the molten region. What is more puzzling is why a similar hysteresis is not found for the cylinder former, for which the critical

stresses for initial alignment and realignment are statistically indistinguishable; thermodynamically, the order-disorder transition is expected to be first order [42] for both morphologies. However, as noted in Fig. 7, even for the cylinder former, the quality of fit could be improved by allowing for a higher σ_c in the second shear. It may simply be that the stress required to nucleate a disordered region is much lower in the cylinder case, leading to only a slight enhancement of σ_c for realignment versus initial alignment, but additional work with other polymers will be required for a conclusive assessment.

IV. CONCLUSIONS

The melting-recrystallization model proposed for shear alignment of both sphere-forming and cylinder-forming block-copolymer thin films was critically tested using a geometry that allowed direct control over the angle difference between the initial grain orientation and the shear direction, as well as the shear stress. First, we confirmed that the cylinder-forming PS-PEP 4/13 can be described by the same model developed for the sphere-forming PS-PEP 3/23 by conducting single-shear experiments from an initially polygrain orientation and imaging larger areas using moiré interference patterns. Once sheared a second time into a new orientation, the alignment of the cylinder-forming block-copolymer thin film is satisfactorily captured by the melting-recrystallization model using the same material parameters. Alignment by double shearing the sphere-forming block-copolymer thin film, however, showed poor quantitative agreement with model calculations based on the parameters derived from shearing an initially polygrain specimen. Adjusting the model's critical stress (σ_c), related to the amount of energy needed to facilitate alignment, to a higher value for the second shearing step resulted in much better agreement. The cause of this increased stress is believed to be the need to nucleate a molten region within the monodomain, thereby generating grain boundaries where dissolution and reformation of the microdomains occurs.

ACKNOWLEDGMENTS

This work was supported by the National Science Foundation (MRSEC Program) through the Princeton Center for Complex Materials (Grant No. DMR-0819860).

[1] S. B. Darling, Prog. Polym. Sci. **32**, 1152 (2007).
[2] P. G. de Gennes and J. Prost, *The Physics of Liquid Crystals* (Clarendon Press, Oxford, 1993).
[3] I. W. Hamley, J. Phys.: Condens. Matter **13**, R643 (2001).
[4] J. Ericksen, Arch. Ration. Mech. Anal. **4**, 231 (1959).
[5] J. L. Ericksen, Phys. Fluids **9**, 1205 (1966).
[6] F. M. Leslie, Q. J. Mech. Appl. Math. **19**, 357 (1966).
[7] F. M. Leslie, Arch. Ration. Mech. Anal. **28**, 265 (1968).
[8] O. Parodi, J. Phys. (Paris) **31**, 581 (1970).
[9] D. M. Boudreau, H. H. Winter, C. P. Lillya, and R. S. Stein, Rheol. Acta **38**, 503 (1999).
[10] B. Van Horn, D. Boudreau, and H. H. Winter, Rheol. Acta **42**, 585 (2003).
[11] B. L. Van Horn and H. H. Winter, Rheol. Acta **39**, 294 (2000).
[12] I. W. Hamley, *The Physics of Block Copolymers* (Oxford University Press, Oxford, 1998).
[13] Z.-R. Chen and J. A. Kornfield, Polymer **39**, 4679 (1998).
[14] C. Daniel, I. W. Hamley, W. Mingvanish, and C. Booth, Macromolecules **33**, 2163 (2000).
[15] J. A. Pople, I. W. Hamley, J. P. A. Fairclough, A. J. Ryan, and C. Booth, Macromolecules **31**, 2952 (1998).
[16] K. Luo and Y. Yang, Polymer **45**, 6745 (2004).
[17] H. Wang, M. C. Newstein, M. Y. Chang, N. P. Balsara, and B. A. Garetz, Macromolecules **33**, 3719 (2000).
[18] D. L. Polis, S. D. Smith, N. J. Terrill, A. J. Ryan, D. C. Morse, and K. I. Winey, Macromolecules **32**, 4668 (1999).
[19] L. Qiao, K. I. Winey, and D. C. Morse, Macromolecules **34**, 7858 (2001).
[20] G. H. Fredrickson, J. Rheol. **38**, 1045 (1994).
[21] J. M. Sebastian, W. W. Graessley, and R. A. Register, J. Rheol. **46**, 863 (2002).
[22] J. M. Sebastian, C. Lai, W. W. Graessley, and R. A. Register, Macromolecules **35**, 2707 (2002).
[23] J. M. Sebastian, C. Lai, W. W. Graessley, R. A. Register, and G. R. Marchand, Macromolecules **35**, 2700 (2002).
[24] M. J. Fasolka and A. M. Mayes, Annu. Rev. Mater. Res. **31**, 323 (2001).
[25] R. A. Segalman, Mater. Sci. Eng. R. **48**, 191 (2005).
[26] G. E. Stein, E. W. Cochran, K. Katsov, G. H. Fredrickson, E. J. Kramer, X. Li, and J. Wang, Phys. Rev. Lett. **98**, 158302 (2007).
[27] D. E. Angelescu, J. H. Waller, D. H. Adamson, P. Deshpande, S. Y. Chou, R. A. Register, and P. M. Chaikin, Adv. Mater. **16**, 1736 (2004).
[28] V. Pelletier, D. H. Adamson, R. A. Register, and P. M. Chaikin, Appl. Phys. Lett. **90**, 163105 (2007).
[29] D. E. Angelescu, J. H. Waller, R. A. Register, and P. M. Chaikin, Adv. Mater. **17**, 1878 (2005).
[30] M. W. Wu, R. A. Register, and P. M. Chaikin, Phys. Rev. E **74**, 040801(R) (2006).
[31] Some previous reports employed a similar model wherein T^*_{ODT} possessed a quadratic dependence on σ [27,28] rather than the linear dependence employed here and in Ref. [30]. The quadratic dependence should hold at the lowest shear rates due to requirements of analyticity and symmetry. However, the coupling of the microdomains to the shearing field should occur quickly and can cause this relationship to become linear as shear rate and thus stress is increased, especially for high molecular weight polymers [A. I. Nakatani *et al.*, J. Chem. Phys. **104**, 1589 (1996)]. As a practical matter, it is difficult to determine the precise functional form of T^*_{ODT} from the data presented here. Indeed, we have refit all the data using a quadratic dependence of T^*_{ODT} on σ and while the values of σ_c necessarily differ, the general quality of the fits is similar. Most impor-

tantly, the finding presented herein that the cylinder-forming diblock can be satisfactorily described by a single value of σ_c (whether for alignment from a polygrain structure or realignment of the oriented structure), while the sphere-forming diblock requires a higher σ_c for realignment than initial alignment, is independent of the functional form assumed for T^*_{ODT}.

[32] C. Harrison, Z. Cheng, S. Sethuraman, D. A. Huse, P. M. Chaikin, D. A. Vega, J. M. Sebastian, R. A. Register, and D. H. Adamson, Phys. Rev. E **66**, 011706 (2002).

[33] A. P. Marencic, M. W. Wu, R. A. Register, and P. M. Chaikin, Macromolecules **40**, 7299 (2007).

[34] D. E. Angelescu, C. K. Harrison, M. L. Trawick, R. A. Register, and P. M. Chaikin, Phys. Rev. Lett. **95**, 025702 (2005).

[35] D. E. Angelescu, J. H. Waller, D. H. Adamson, R. A. Register, and P. M. Chaikin, Adv. Mater. **19**, 2687 (2007).

[36] J. L. Adams, D. J. Quiram, W. W. Graessley, R. A. Register, and G. R. Marchand, Macromolecules **31**, 201 (1998).

[37] A block copolymer's T_{ODT} in a thin film can differ from its T_{ODT} in bulk because of substrate and free-surface effects. The T_{ODT} for a film of PS-PEP 3/23 containing a single layer of spherical microdomains was previously measured to be 125 °C [34] versus the bulk value of $T_{\mathrm{ODT}}=121\pm2$ °C. We were unable to measure the thin film T_{ODT} for the PS-PEP 4/13 because of the rapid formation of large grains, but we expect it to be similarly close to the bulk T_{ODT} since it has the same block chemistry and wetting conditions as the sphere former. We chose to consistently use the bulk T_{ODT} values because they are available for both polymers, but as a practical matter, using a slightly different value for T_{ODT} in our fits would simply change the best-fit value of the critical stress slightly (not beyond our quoted uncertainties) and would not affect our discussion or conclusions.

[38] Y.-R. Hong, D. H. Adamson, P. M. Chaikin, and R. A. Register, Soft Matter **5**, 1687 (2009).

[39] M. W. Wu, Ph.D. thesis, Princeton University, 2005.

[40] A. Hexemer, G. E. Stein, E. J. Kramer, and S. Magonov, Macromolecules **38**, 7083 (2005).

[41] J. C. Crocker and D. G. Grier, J. Colloid Interface Sci. **179**, 298 (1996).

[42] D. A. Hajduk, S. M. Gruner, S. Erramilli, R. A. Register, and L. J. Fetters, Macromolecules **29**, 1473 (1996).

[43] See supplementary material at http://link.aps.org/supplemental/10.1103/PhysRevE.81.011503 for color-scale versions of figures.